

GHz properties of magnetophoretically aligned iron-oxide nanoparticle doped polymers

Ferruccio Pisanello, Rosa De Paolis, Daniela Lorenzo, Pablo Guardia, Simone Nitti,

Giuseppina Monti, Despina Fragouli, Athanassia Athanassiou, Luciano Tarricone,

Liberato Manna, Massimo De Vittorio, Luigi Martiradonna

Supporting Information

Section	Title	Page
I	Synthesis of Iron oxide nanoparticles	1
II	Magnetic Characterization, Table S1	2
III	Measurement of the dielectric permittivity and magnetic permeability, Figure S1	3
IV	Cluster size probability estimation, Figure S2	5

I- Synthesis of Iron oxide nanoparticles

The syntheses of iron oxide nanoparticles were carried out using commercially available reagents. Iron(III) oxide hydrated (catalyst grade 30–50 mesh), 1-Octedecene(90%), Oleic acid (90%), Toluene 2-Propanol were purchased from Sigma-Aldrich and used as received.

- 15 ± 1 nm (D~15nm): In a three neck flask, 2 mmol of Iron(III) oxide hydrated and 8.5 mmol of oleic acid were mixed in 5g of 1-octedecene. The solution was degassed and stirred at room temperature for 30 minutes. Later the temperature was allowed to increase up to reflux temperature (320°C) and kept at this temperature for 1 hour under a nitrogen flow. After cooling down, particles were washed by adding 10 mL of 2-propanol followed by centrifugation at 4000 rpm for 15 minutes. The final product was dispersed in toluene (0.316 M of iron atoms in toluene solution) and named D~15nm.

- 29 ± 2 nm (D~29nm): A solution containing 2 mmol of Iron(III) oxide hydrated, 12 mmol of oleic acid and 5g of 1-octedecene was mixed and stirred at room temperature. After degassing for 30 minutes, the solution was heated up to reflux temperature (320°C) and kept at this temperature for 1 hour under a nitrogen flow. The solution was then cooled down and particles were collected by adding 10 mL of 2-propanol followed by centrifugation at 4000 rpm for 15 minutes. The final product was dispersed in toluene at a concentration of 0.238 M of iron atoms and named D~29nm.

II- Magnetic Characterization:

Magnetic properties of IONPs were performed in a commercial SQUID magnetometer Quantum Design MPMSXL. For sample preparation, 25 μ l of the above mentioned solutions were dropped and dried into a Teflon film. After solvent evaporation the dried powder was enwrapped and measured. Zero Field Cool and Field Cool curves (ZFC-FC) were measured from 5K up to 400 K under a magnetic field of 25 Oe using a heating and cooling rate of 1.5K min. Hysteresis loops were measured up to 7 Tesla at two different temperatures (5K and 300 K). In the high magnetic field region, they can be fitted to $M(H) = M_s + \chi_d H$, being M_s the zero-field saturation magnetisation and χ_d the high-field differential susceptibility. M_s is obtained by fitting the high field branches (H higher than 20 000 Oe) of the hysteresis loop. Coercive fields (H_c^\pm) were evaluated as the field in which the magnetization becomes 0 and the final coercive field calculated as;

$$H_C = \frac{|H_C^- + H_C^+|}{2}$$

H_c^- represents the coercive field for the negative branch while H_c^+ belongs to the positive one. The exchange field H_{Ex} , which takes into account the exchange interactions, was calculated as:

$$H_{Ex} = \frac{|H_C^- - H_C^+|}{2}$$

D 15 nm	M_s (emu/g _{Fe})	H_c^+ (Oe)	H_c^- (Oe)	H_c (Oe)	H_{ex} (Oe)
5 K	67	910	1200	1055	145
300 K	58	-11	11	11	-
D 29 nm	M_s (emu/g _{Fe})	H_c^+ (Oe)	H_c^- (Oe)	H_c (Oe)	H_{ex} (Oe)
5 K	64	1378	1793	1585	207
300 K	64	-10	10	10	-
Standard Samples 17 nm*	M_s (emu/g _{Fe})	H_c^+ (Oe)	H_c^- (Oe)	H_c (Oe)	H_{ex} (Oe)
5 K	120	370	370	-	-
300 K	n.d.	n.d.	n.d.	n.d.	n.d.

Table S1: Summary of the magnetic properties. Saturation magnetization (M_s), coercive fields (H_c^- , H_c^+ and H_c) and exchange field (H_{ex}) at 5 K and 300 K for D~15nm and D~29nm samples (*Journal of Magnetism and Magnetic Materials 316 (2007) e756–e759 doi:10.1016/j.jmmm.2007.03.085)

III- Measurement of the dielectric permittivity and magnetic permeability

s

This paragraph briefly describes the method used to evaluate complex dielectric permittivity and magnetic permeability of the PNCs investigated in this work. For the sake of generality and to avoid heavy notation, in this paragraph the dielectric permittivity and magnetic permeability of the nanocomposite under test will be referred to as $\varepsilon_{2r} = \varepsilon'_{2r} - j\varepsilon''_{2r}$ and $\mu_{2r} = \mu'_{2r} - j\mu''_{2r}$. The used electromagnetic setup is schematized in Figure S1(a): a coplanar waveguide (CWG) with finite ground planes (characteristic impedance 50 Ω , center conductor width $s \sim 2.23$ mm, gaps width $w \sim 233$ μm , ground planes width $g \sim 6.7$ mm, see sketch in Figure S1(c)) is connected to a Vector Network Analyzer (VNA, HP 08753ES) through an universal test fixture (Anritsu 3680-20), and the nanocomposite is positioned on the coplanar substrate. At each measurement, the frequency of the incident electromagnetic wave is scanned in the range 0.5 GHz and 2.5 GHz while magnitude and phase of scattering coefficients at Port 1 and Port 2 are recorded. ε_{2r} and μ_{2r} are estimated using the post-measurement analysis described below.

As shown in Figure S1(a) and (b) the CWG can be divided in three different electromagnetic regions: two composed by CWGs with known dielectric substrate and one with an additional overlay layer, i.e. the nanocomposite under test. From CWG conformal mapping approach, each of these sections can be characterized by an effective permittivity and an effective permeability, hereafter referred to as $\varepsilon_{\text{rCWG}}$ and μ_{rCWG} for the bare CWG sections and $\varepsilon_{\text{reff}}$ and μ_{reff} for the region containing the nanocomposite. $\varepsilon_{\text{reff}}$ and μ_{reff} are linked to permeability and permittivity of each layer composing the structure by the following relations [B. Kang, J. Cho, C. Cheon, Y. Kwon, IEEE Microw. Wirel. Co. **2005**, 15, 381–383; R.N. Simons, Simons, *Coplanar waveguide circuits, components, and systems*, Wiley Online, Library, **2001**]:

$$\begin{aligned}\varepsilon'_{\text{reff}} &= q_1 \varepsilon'_{1r} + q_2 \varepsilon'_{2r} + q_3 \varepsilon'_{3r} + q_b \\ \varepsilon''_{\text{reff}} &= q_1 \varepsilon''_{1r} + q_2 \varepsilon''_{2r} + q_3 \varepsilon''_{3r} \\ \frac{1}{\mu'_{\text{reff}}} &= q_1 \frac{1}{\mu'_{1r}} + q_2 \frac{1}{\mu'_{2r}} + q_3 \frac{1}{\mu'_{3r}} + q_b \\ \frac{\mu''_{\text{reff}}}{(\mu'_{\text{reff}})^2} &= q_1 \frac{\mu''_{1r}}{(\mu'_{1r})^2} + q_2 \frac{\mu''_{2r}}{(\mu'_{2r})^2} + q_3 \frac{\mu''_{3r}}{(\mu'_{3r})^2}\end{aligned}\tag{S1}$$

where ε_{ir} and μ_{ir} are assigned to the materials composing the setup in Figure S1(c). q_i are coefficients depending on CWG geometry as follows:

$$\begin{aligned}q_1 &= \frac{1}{2} \frac{K(k)}{K(k')} \left[\frac{K(k'_1)}{K(k_1)} - \frac{K(k'_2)}{K(k_2)} \right] \\ q_2 &= \frac{1}{2} \frac{K(k)}{K(k')} \frac{K(k'_2)}{K(k_2)} \\ q_3 &= \frac{1}{2} \frac{K(k)}{K(k')} \frac{K(k'_3)}{K(k_3)} \\ q_b &= 1 - \frac{1}{2} \frac{K(k)}{K(k')} \left[\frac{K(k'_1)}{K(k_1)} + \frac{K(k'_3)}{K(k_3)} \right]\end{aligned}$$

where

$$\frac{K(k)}{K(k')} = \frac{\ln\left(2\frac{1+\sqrt{k}}{1-\sqrt{k}}\right)}{pi} \quad \text{if } 1/\sqrt{2} \leq k \leq 1$$

$$\frac{K(k)}{K(k')} = \frac{pi}{\ln\left(2\frac{1+\sqrt{k'}}{1-\sqrt{k'}}\right)} \quad \text{otherwise}$$

$$\frac{K(k_i)}{K(k'_i)} = \frac{\ln\left(2\frac{1+\sqrt{k_i}}{1-\sqrt{k_i}}\right)}{pi} \quad \text{if } 1/\sqrt{2} \leq k_i \leq 1$$

$$\frac{K(k_i)}{K(k'_i)} = \frac{pi}{\ln\left(2\frac{1+\sqrt{k'_i}}{1-\sqrt{k'_i}}\right)} \quad \text{otherwise}$$

$$k_i = \frac{\sinh\left(\frac{\pi C}{2h_i}\right)}{\sinh\left(\frac{\pi B}{2h_i}\right)} \sqrt{\frac{\sinh^2\left(\frac{\pi B}{2h_i}\right) - \sinh^2\left(\frac{\pi A}{2h_i}\right)}{\sinh^2\left(\frac{\pi C}{2h_i}\right) - \sinh^2\left(\frac{\pi A}{2h_i}\right)}}$$

$$k'_i = \sqrt{1 - k_i^2}$$

$$k = \frac{C}{B} \sqrt{\frac{B^2 - A^2}{C^2 - A^2}}$$

$$k' = \sqrt{1 - k^2}$$

$$A = \frac{s}{2}$$

$$B = \frac{s + 2w}{2}$$

$$C = 2B + 2g$$

ϵ_{reff} and μ_{reff} can instead be estimated directly from the measured scattering coefficients by using the transmission line representation shown in Figure S1(b) and taking into account the phase delay introduced by the two bare CWG sections (each long l) [W. Barry, IEEE T. Microw. Theory **1986**, 34, 80–84.]:

$$kd = \frac{\text{acos}\left(e^{-j4k_{CWG}l} + S_{21}^2 - S_{11}^2\right)}{e^{-j2k_{CWG}l} S_{21}}$$

$$\Gamma = \frac{S_{11}}{e^{-j2k_{CWG}l} - S_{21}e^{-jkd}}$$

$$\epsilon_{\text{reff}} = \frac{k}{k_{CWG}} \frac{1 - \Gamma}{1 + \Gamma} \epsilon_{rCWG}$$

$$\mu_{\text{reff}} = \frac{k}{k_{CWG}} \frac{1 + \Gamma}{1 - \Gamma} \mu_{rCWG} \quad (\text{S2})$$

where $k_{CWG} = \omega / (c\sqrt{\epsilon_{rCWG}\mu_{rCWG}})$, Γ is the reflection coefficient at the interface A1 or A2, kd is the electrical length of the region containing the material under test, and S_{xy} are scattering coefficients as exciting at port y and collecting reflected or transmitted signal at port x .

Equations (S2) and (S1) thus allow to compute $\epsilon_{2r} = \epsilon'_{2r} - j\epsilon''_{2r}$ and $\mu_{2r} = \mu'_{2r} - j\mu''_{2r}$ from a direct measurement of scattering parameters S_{11} and S_{21} , or S_{12} and S_{22} . A detailed discussion on measurement errors introduced by this method is given in ref. [Pisanello, F. et al., *Microelectron. Eng.* **2012**, *In Press* <http://dx.doi.org/10.1016/j.mee.2012.11.013>].

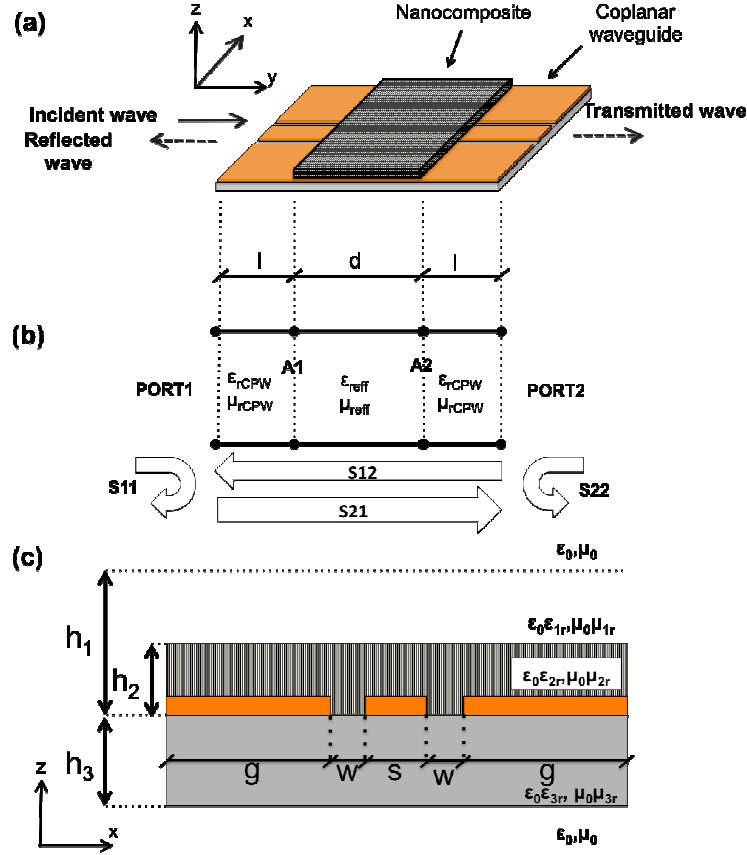


Figure S1. Electromagnetic setup used to characterize the nanocomposite under test. Panel (a) Sketch of the coplanar waveguide configuration used to measure scattering coefficients. **Panel (b)** Transmission line model exploited to compute the effective dielectric permittivity and magnetic permeability of the CWG section containing the material under test. **Panel (c)** Geometrical configuration of the CWG.

IV- Cluster size probability estimation

This paragraph illustrates the method used to determine the probability to have a cluster area a bigger than a given value A shown in Figure 2(f). Transmission microscope images were acquired by a Nikon microscope (model “Eclipse”) equipped with a color CCD camera (see Figures S2(a) and (b)). Obtained images were converted in grey scale and particles clusters identified by a segmentation process based on the *particle analysis* function of the software ImageJ [<http://rsb.info.nih.gov/ij/>]. Typical outputs of the segmentation procedure are displayed in Figures S2(c) and (d). The area of each identified cluster was measured and the number of clusters bigger than a given value A were computed by using a simple Matlab script. Graphs reported in Figure 2(f) were computed for A ranging from the smallest to the biggest cluster area and $P(a>A)$ obtained through a normalization to the number of identified clusters.

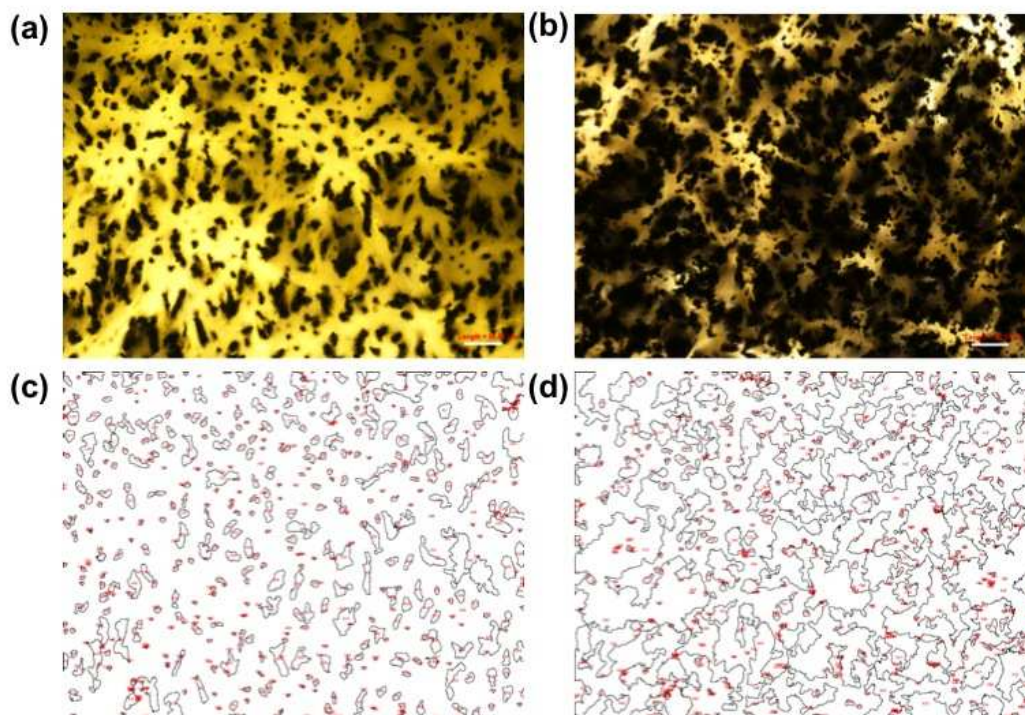


Figure S2. Image Segmentation. Panels (a,b) Top view of aligned NPs samples for NPs diameters of $D \sim 29\text{nm}$ and $D \sim 15\text{nm}$, respectively. Scale bars are $50\mu\text{m}$. Panels (c,d) Results of the segmentation performed on images reported in panels (a) and (b), respectively.